Anal. Chem. **1997,** *69,* 4627−4633

Current Rectification at Quartz Nanopipet Electrodes

Chang Wei† and Allen J. Bard*

Department of Chemistry and Biochemistry, The University of Texas at Austin, Austin, Texas 78712

Stephen W. Feldberg

Department of Applied Science, Brookhaven National Laboratory, Upton, Long Island, New York 11973

Ag/AgCl reference electrodes fabricated from pulled quartz tubes with orifice radii of 20 nm to 20 μm were characterized in KCl solutions of different concentrations by cyclic voltammetry. Linear current−voltage ($i-V$) dependence was observed with micropipet electrodes (with micrometer-sized tips) with the same concentration (0.01−1 M) of KCl inside and outside the pipet, but current rectification was found at nanopipet electrodes at KCl concentrations of ≤0.1 M (with nanometer-sized tips). This is attributed to formation of a diffuse electrical double layer within the tip orifice. The effects of electrode size, electrolyte concentration, and solution pH on the nonlinear $i-V$ behavior of these electrodes were investigated. A model for the observed behavior shows the rectification to be caused by the permselectivity in the tip region and the geometric asymmetry of the tip orifice. This phenomenon may be important in studies of ion transport in charged channels and porous membranes.

Pipet-based electrodes have been used for a wide range of applications, especially in performing electrochemical measurements with high spatial resolution. Micropipet ion-selective electrodes (ISEs), which were developed for potentiometric determination of the local activity of different ions, are particularly useful in the life sciences for measurement of intracellular and extracellular ion activities in living cells.[1] Miniaturization of the electrode body has made possible the fabrication of pipet-based ISEs with tip diameters of micrometer and submicrometer dimensions. Moreover, several scanning probe techniques based on micropipet electrodes have been developed to obtain topographic and chemical information about a sample substrate by scanning the micropipet probe in close proximity to the target. For example, scanning ion conductance microscopy, which uses an electrolyte-filled Ag/AgCl micropipet electrode as the probe, was introduced to image the topography of surfaces with submicrometer spatial resolution,[2,3] and a form of scanning electrochemical microscopy (SECM; scanning ion-selective potentiometric microscopy) was developed to map local concentration profiles of various ions around micrometer-sized objects using micropipet-based ISEs.[4−6]

One of the challenges in using pipet-based electrodes for electrochemical measurements is improved spatial resolution, and the fabrication of even smaller electrodes (nanometer-sized probes) is needed to achieve this. The fabrication of nanopipets has been made possible by the use of microprocessor-controlled pipet pullers with laser heating of quartz tubes to produce orifice diameters of a few tens of nanometers,[7] and nanopipet electrodes can be constructed using these and an electrolyte filling. In the course of applying nanopipet electrodes to high-resolution SECM measurements and the modeling of their behavior, we characterized the electrochemical properties of these electrodes by studying their current vs potential ($i-V$) response. We found that, at low concentrations of electrolyte, apparently symmetrical cells with the same electrolyte in both compartments produced nonlinear $i-V$ dependencies when one of the electrodes was enclosed by a nanopipet, in contrast to the linear $i-V$ relation observed with a micropipet salt bridge. We ascribe these effects to a combination of permselectivity effected by surface charge that can exist at the quartz/electrolyte interface[8] and a geometric effect caused by the asymmetry of the orifice. These phenomena were investigated by exploring the effects of electrode size, electrolyte concentration, and solution pH on the $i-V$ dependence.

EXPERIMENTAL SECTION

KCl (reagent grade) and HCl (36.5−38%) were obtained from J. T. Baker (Phillipsburg, NJ) and E. M. Sciences (Fort Washington, NJ), respectively, and were used as received. Silver wires (0.25-mm diameter, 99.99%) were purchased from Aldrich (Milwaukee, WI), and quartz tubes (1.0-mm o.d., 0.7-mm i.d.) were obtained from Sutter Instruments (Novato, CA). All experiments were performed in aqueous solutions prepared from deionized Milli-Q water (Millipore Corp.).

The fabrication of nanopipet electrodes is described in detail elsewhere.[7] Briefly, nanometer-sized capillaries were pulled

† Current address: Corporate Research and Development, General Electric Company, P.O. Box 8, Schenectady, NY 12301

(1) Ammann, D. *Ion Selective Microelectrodes: Principles, Design and Application*; Springer-Verlag: New York, 1986.
(2) Prater, C. B.; Hansma, P. K.; Tortonese, M.; Quate, C. F. *Rev. Sci. Instrum.* **1991**, *62*, 2634.
(3) Hansma, P. K.; Marti, O.; Gould, S. A. C.; Prater, C. B. *Science* **1989**, *243*, 641.
(4) Wei, C.; Bard, A. J.; Nagy, G.; Toth, K. *Anal. Chem.* **1995**, *67*, 1346.
(5) Toth, K.; Nagy, N.; Wei, C.; Bard, A. J. *Electroanalysis* **1995**, *7*, 801.
(6) Horrocks, B. R.; Mirkin, M. V.; Pierce, D. T.; Bard, A. J.; Nagy, N.; Toth, K. *Anal. Chem.* **1993**, *65*, 1213.
(7) User's Manual for Laser Puller Model P-2000; Sutter Instruments, Novato, CA, 1993.
(8) Lavallée, M.; Szabo, G. In *Glass Microelectrodes*; Lavallée, M., Schanne, O. F., Hébert, N. C., Eds.; Wiley: New York, 1969; Chapter 6. These authors described how charges on the wall of a narrow glass capillary give rise to a diffuse double layer and affect the tip potential and conductivity. Permselectivity in a very narrow capillary at low electrolyte concentrations is a logical consequence of their model.

S0003-2700(97)00551-9 CCC: $14.00

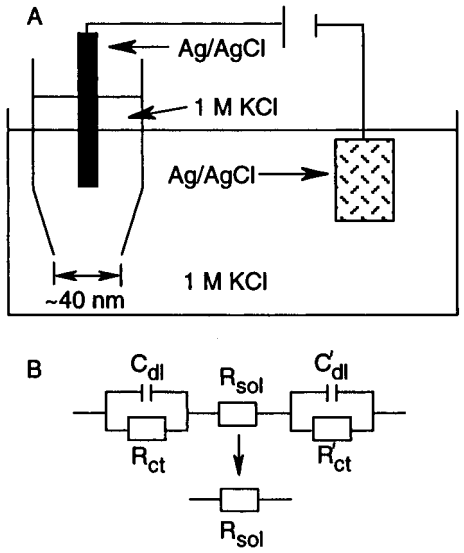

Figure 1. (A) Typical setup for electrochemical measurements using a Ag/AgCl nanopipet electrode. (B) Equivalent circuit representing the electrochemical processes described in eq 1.

directly from clean quartz tubes using a microprocessor-controlled CO_2 laser-based puller (Model P-2000, Sutter Instruments). The geometry of the capillaries (i.e., tip length and diameter) was controlled by selection of the puller parameters. In the experiments described here, the smallest tip diameters were a few tens of nanometers and the tip length was ~9 mm. Tip diameters were determined by measuring the resistance of the solution in the capillary, which is dominated by the drawn section.[4] These were consistent with larger diameter capillaries that could also be imaged by scanning electron microscopy and with the nominal tip diameters for quartz capillaries given by Sutter Instruments for the pulling parameters employed. The nanometer-sized capillaries were then back-filled with electrolyte (e.g., 0.1 M KCl) using a micropipet syringe (WPI, Sarasota, FL) to allow the introduction of the solution into the end of the tip by capillary action. After the careful removal of air remaining inside the capillaries, a Ag/AgCl wire was inserted from the back to complete the electrode.

A two-electrode system was used in the experiments and a typical setup is shown in Figure 1A, in which a Ag/AgCl nanopipet electrode served as the working electrode and another Ag/AgCl electrode was placed in bulk solution as an auxiliary/reference electrode (the current passed by the nanopipet electrodes is too small to polarize the reference electrode). In all cases, the nanopipet electrode was filled with the same electrolyte as the bulk solution. Cyclic voltammetric experiments were carried out with an EI-400 bipotentiostat (Ensman Instruments, Bloomington, IN) in conjunction with a PC.

RESULTS AND DISCUSSION

Measurements at Nanopipets. When a dc voltage is applied between the two Ag/AgCl electrodes shown in Figure 1A, the following process occurs at the electrode/electrolyte interface:

$$AgCl + e \rightleftarrows Ag + Cl^- \qquad (1)$$

Figure 1B shows the equivalent circuit representing this electrochemical cell. Because both Ag/AgCl electrodes have large surface areas relative to the nanometer-sized aperture of the pipet and the charge-transfer processes in eq 1 are rapid, we can neglect the impedance contributions from the double-layer capacitance (C_{dl}, C_{dl}') and the charge-transfer resistance of the electrodes (R_{ct}, R_{ct}'), and the equivalent circuit can be simplified to one in which the current is governed by the solution resistance, R_{sol}. Thus, a linear $i-V$ relation is expected for a nanopipet electrode with known geometry since the solution resistance is independent of i. Figure 2A shows a typical cyclic voltammogram of a Ag/AgCl nanopipet electrode in 1 M KCl solution. For these conditions, the current at the electrode is a linear function of voltage, and thus, the solution resistance can be extracted from the slope of the $i-V$ curve. However, cyclic voltammograms of these electrodes in less concentrated electrolytes showed unexpected nonlinear $i-V$ features (Figure 2B,C). In contrast to curve A (1 M KCl), both curves B and C (0.1 M and 0.01 M KCl, respectively) exhibit asymmetric $i-V$ curves in which the current in the cathodic direction is larger than that in the anodic direction. In all cases, voltages are given as that of the nanopipet electrode vs the Ag/AgCl electrode in bulk solution, and anodic and cathodic refer to the processes at the nanopipet electrode. The more dilute the electrolyte used, the more asymmetric are the features observed. On the other hand, this nonlinear current−potential dependence was not observed for larger sized pipet electrodes (i.e., micrometer-sized electrodes) even with the same less concentrated electrolytes (Figure 3). We believe there are two phenomena operating here: (1) permselectivity effected by charges on the inner surface of the nanopipet and controlled by the nature of the diffuse double layer associated with those charges; and (2) once permselectivity has modified the transference numbers for the mobile ions within the nanopipet so that they are different from the those in the bulk, concentration polarization occurs at the ends of the nanopipet.

Diffuse Double-Layer (ddl) Effects. An ionic electrical double layer forms at the interface between quartz and an electrolyte solution because specific ionic adsorption on the quartz or dissociation of protons from surface groups leads to a surface charge that is compensated by a diffuse ionic layer in solution.[8] Frequently the surface charge on quartz is dominated by H^+ or OH^- adsorption and thus depends on the solution pH. The isoelectric point, the pH effecting zero net surface charge, is generally within the pH range of 1−4 for various types of SiO_2 materials.[9] Thus, a quartz surface will be negatively charged in a KCl solution of pH 6.8, which is greater than the isoelectric point. Under these conditions, the ddl near the surface contains an excess of cations (K^+) and a deficiency of anions (Cl^-). Figure 4 is a simplified representation of the ddl formed at the end of a quartz-based nanopipet electrode. Note that only the portion associated with the inner surface of the pipet is presented. With the configuration shown in Figure 1A, one expects that the current flow between the two electrodes will be dominated by ion transport through the pipet opening, depending on the thickness of the ddl relative to the size of the electrode tip. For example, when the ddl thickness is comparable to the diameter of a nanometer-sized tip, the current (ion flux) must pass through the diffuse layer and the electrostatic interaction between ionic species and surface charges will affect ion transport properties. On the other hand, if the ddl thickness is negligible compared to the tip diameter, the ddl will not affect ion movement, because most of the ions

(9) Parks, G. A. *Chem. Rev.* **1965**, *65*, 177.

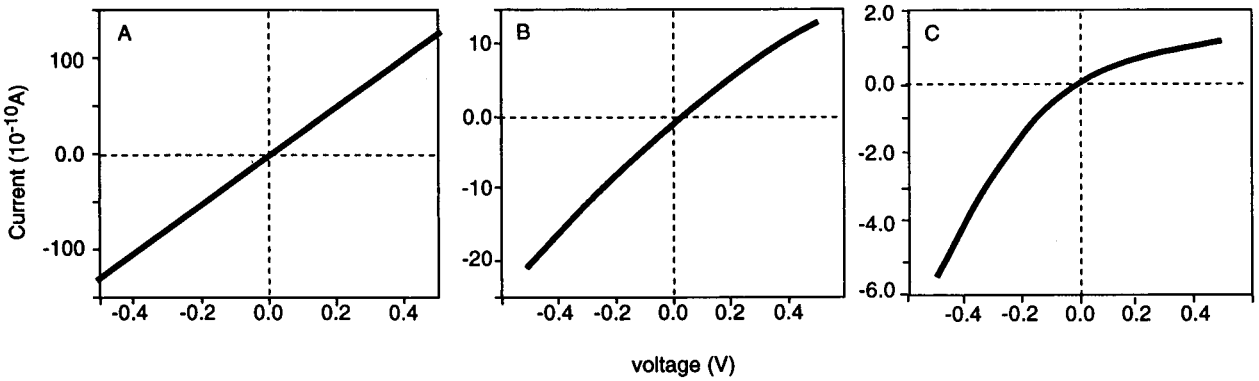

Figure 2. Cyclic voltamograms of Ag/AgCl nanopipet electrodes (~20 nm radius) in (A) 1.0, (B) 0.1, and (C) 0.01 M KCl. Scan rate, 20 mV/s. The potential axis represents that of the Ag/AgCl electrode in the pipet vs another in bulk solution with the same KCl concentration.

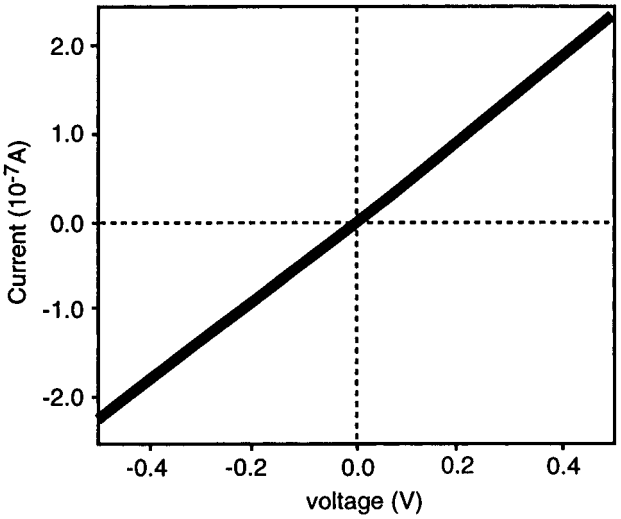

Figure 3. Typical cyclic voltammogram of 20-μm-diameter Ag/AgCl micropipet electrode in 0.01 M KCl. Scan rate, 20 mV/s.

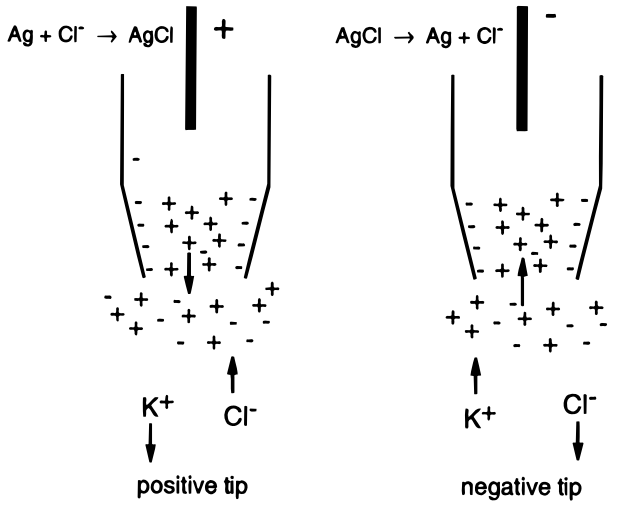

Figure 4. Schematic for an electrical double layer formed at the inner surface of a quartz-based pipet electrode in KCl solution. The quartz surface is assumed to be negatively charged, and the arrows indicate the directions of ion movement while the corresponding potential is applied to the nanopipet electrode.

migrate through the electrically neutral (bulk composition) zone of the electrolyte. Thus the $i-V$ characteristics of nanopipet electrodes will be strongly affected by the ddl thickness at the quartz surface of the electrode orifice.

An estimate of the characteristic thickness of the diffuse layer at planar electrodes can give useful information about the effect of the ddl on ion transport. The thickness of the ddl (δ) at a planar surface for a 1:1 electrolyte is given by[10]

$$\delta = 1/\kappa = (2n^{\circ}z^2e^2/\epsilon\epsilon_0 kT)^{-1/2} \qquad (2)$$

where n° is the concentration of species of charge z in a phase of dielectric constant ϵ at temperature T, and e, ϵ_0, and k are the electronic charge, permittivity of free space, and Boltzmann constant, respectively. At 25 °C, for aqueous solutions this can be written as

$$1/\kappa = 3.1 \times 10^{-8}/c^{*1/2}\ (\text{cm}) \qquad (3)$$

where c^* is the concentration (in mol/L).

The ddl thickness is significantly reduced with an increase of electrolyte concentration; e.g., the characteristic thickness of the ddl is about 3, 1, and 0.3 nm in 0.01, 0.1, and 1 M KCl solutions, respectively.[10] Thus, for a 20-nm-diameter electrode, the area within $1/\kappa$ at the orifice represents 51, 19, and 6% of the cross-sectional area for the corresponding electrolyte concentrations. However, for a pipet electrode with a diameter of 20 μm, only 0.6% of the cross-sectional area at the opening is occupied by the ddl even in 0.01 M KCl; i.e., 99.4% of the electrode area is an electrically neutral zone. Clearly, the more cross-sectional area taken by the ddl, the greater the effect on ion transport through the opening. Consider a 20-nm-pipet electrode filled with 0.01 M KCl electrolyte, as shown schematically in Figure 4. The double layer forms across the orifice to compensate the negative charge on the glass so that anions (Cl^-) are excluded from this region. This modifies the usual ionic fluxes of K^+ and Cl^- that occur at the tip during electrolysis. Since the transference numbers of K^+ and Cl^- are both ~0.5, passage of current at the Ag/AgCl electrodes in the usual salt bridge results in about equal fluxes of K^+ and Cl^- to compensate charge.[10] Consider the situation when an anodic process occurs at the nanopipet Ag/AgCl electrode (Figure 4, left). Chloride ion is consumed at the Ag electrode and must be replenished by Cl^- diffusing and migrating to the Ag. However, because of the permselective nature of the orifice, electroneutrality is maintained mainly by K^+ moving out of the

(10) Bard, A. J.; Faulkner, L. R. *Electrochemical Methods: Fundamentals and Applications*; John Wiley & Sons: New York, 1980.

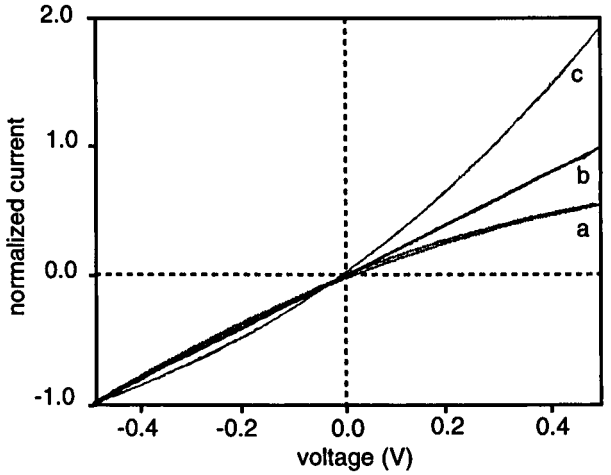

Figure 5. Cyclic voltammograms of nanopipet electrodes (~20 nm radius) in 0.01 M KCl with the addition of (a) 0.1, (b) 0.4, and (c) 1 mM HCl. Current is normalized to the cathodic current at −0.5 V for each electrode. Scan rate, 20 mV/s.

nanopipet. For a cathodic process at the nanopipet, the current flow produces Cl^-, which is compensated mainly by the flow of K^+ into the tip. However, permselectivity by itself does not confer asymmetry in the $i-V$ behavior. For example, the pores in an ion exchange membrane are analogous to that at the nanopipet, yet such membranes generally do not show asymmetrical $i-V$ curves. Asymmetry must arise from either a charge separation at the end of the nanopipet (for example, as in asymmetric phospholipid bilayer membranes[11]) or differences in the limiting transport rates into and out of the tip, as discussed below. For example, when the tip electrode is positive, K^+ moves out of the tip and is limited by a largely linear process constrained by the tip diameter. For a negative tip electrode, K^+ moves in from a hemispherical field outside the tip, is less hindered, and produces a larger current.

Effect of pH. The proposed importance of wall charge can be tested by carrying out experiments at pHs below the isoelectric point. Protonation of surface sites under acidic conditions produces a positive surface largely compensated by chloride ion.[12] Figure 5 shows $i-V$ curves of nanopipet electrodes in 0.01 M KCl electrolyte with HCl added for pH adjustment. The current in Figure 5 has been normalized to a cathodic current at −0.5 V for each electrode. The $i-V$ curves of these nanopipet electrodes show that the nature of the asymmetry depends on pH. In 0.4 mM HCl, a linear $i-V$ dependence is observed (curve b). The results suggest that at this pH the quartz surface is essentially uncharged and thus ion transport through the nanometer opening is not affected. The isoelectric point obtained from Figure 5 is within the range of literature values.[9] In 1.0 mM HCl, however, cyclic voltammograms show current rectification in a direction opposite from the curves in Figure 2. In this case, the current flow is controlled by Cl^- motion and is larger for the hemispherical motion in (positive tip electrode) than linear motion out (negative tip electrode).

Model for Asymmetric Tip Currents. We consider here transport at the tip and show that the asymmetric behavior can be explained by the permselectivity at the tip terminus along with

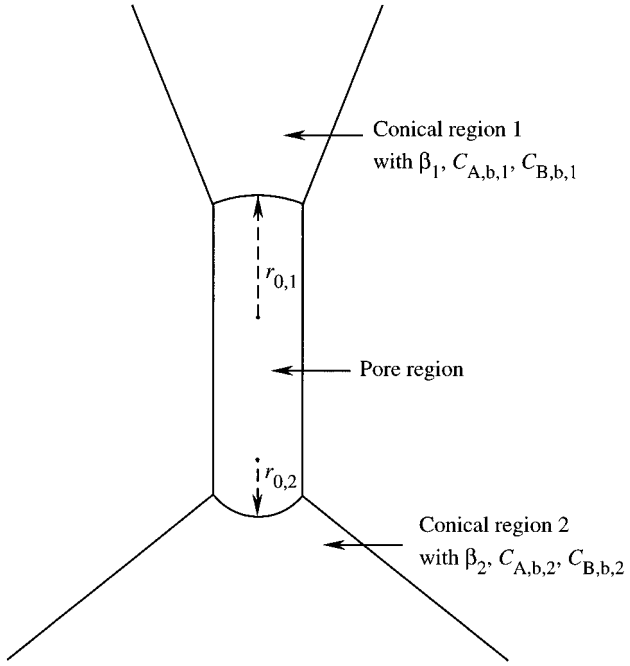

Figure 6. Schematic model of tip. Conical region 1 and conical region 2 are characterized by β_1 and β_2, respectively, the fraction of the full 4π solid angle subtended by the cone. $C_{A,b,1}$ and $C_{B,b,1}$ are the bulk concentrations of species A and B, respectively, in region 1; $C_{A,b,2}$ and $C_{B,b,2}$ are the bulk concentrations in region 2. The access radii to the pore are $r_{0,1}$ and $r_{0,2}$ for regions 1 and 2, respectively.

the geometry at the terminus. A simplified model for the capillary tip, shown in Figure 6, comprises two conical access regions (labeled 1 and 2) linked by a connecting pore which can exhibit some permselectivity.[8] Conical region 1 connects to the upper end of the pore whose access radius is $r_{0,1}$; the conical solid angle segment is characterized by β_1, the fraction of the full 4π solid angle subtended by the cone. Similarly, conical region 2 connects to the lower end of the pore whose access radius is $r_{0,2}$; the conical solid angle segment is characterized by β_2. For generality, we consider an electrolyte composed of A^{z_A} and B^{z_B} with diffusion coefficients of D_A and D_B, respectively, and with bulk concentrations $C_{A,b,1}$ and $C_{B,b,1}$ in region 1 and $C_{A,b,2}$ and $C_{B,b,2}$ in region 2. We will present a general analysis. However, for the experimental case of interest here, $z_A = 1$, $z_B = -1$, $D_A = D_B$, $C_{A,b,1} = C_{A,b,2}$, and $C_{B,b,1} = C_{B,b,2}$. Permselectivity in the pore region is taken into account by considering the fluxes of A and B in this region, f_A and f_B, to be related by

$$f_B = -\alpha f_A \tag{4}$$

where α is a selectivity parameter and where $0 \le \alpha \le \infty$. For total cationic permselectivity, $\alpha \to 0$; for total anionic permselectivity, $\alpha \to \infty$.

The magnitude of α is a function of many factors: D_A, D_B, z_A, and z_B, of course, but with critical modification effected by properties of the pore itself:[8] its dimensions, surface charge density, and associated diffuse double layer (which will also be a function of the ion concentrations). We analyze this system by a simple model that considers the steady-state flux of A and B to partial spheres with radii $r_{0,1}$ and $r_{0,2}$. We assume that the Nernst−Planck equations apply to mass transfer (implying the absence of convection) and that electroneutrality exists throughout the

(11) Coronado, R.; Latorre, R. *Biophys. J.* **1983**, *43*, 231.
(12) Davis, J. A.; James, R. O.; Leckie, J. O. *J. Colloid Interface Sci.* **1978**, *63*, 480.

conical regions. In the context of Figure 6, a positive flux will be considered to be away from the pore. The details of the derivations are presented in the Appendix. The potential drop through conical region 1 (Figure 6) is ΔV_1 deduced by integrating the electric field from $r_1 = r_{0,1}$ to $r_1 = \infty$ (see Appendix):

$$\Delta V_1 = \frac{RT}{z_A pF} \ln\left[1 - \frac{i_1}{i_{\text{lim},1}}\right] \tag{5}$$

where

$$p = \frac{1 - \alpha(D_A/D_B)}{(z_A/z_B) - \alpha(D_A/D_B)} \tag{6}$$

$$\frac{i_1}{i_{\text{lim},1}} = \frac{C_{A,b,1} - C_{A,r_{0,1}}}{C_{A,b,1}} \tag{7}$$

The expression for the current i_1 is (see Appendix)

$$i_1 = -4\pi F \beta_1 r_{0,1} D_A (C_{A,b,1} - C_{A,r_{0,1}}) \frac{[1 - (z_A/z_B)](z_A - \alpha z_B)}{[1 - (\alpha D_A/D_B)]} \tag{8}$$

and the limiting current $i_{\text{lim},1}$ represents the condition when $C_{A,r_{0,1}} \rightarrow 0$.

$$i_{\text{lim},1} = -4\pi F \beta_1 r_{0.1} D_A C_{A,b,1} \frac{[1 - (z_A/z_B)](z_A - \alpha z_B)}{[1 - (\alpha D_A/D_B)]} \tag{9}$$

As long as $0 < i/i_{\text{lim}} \leq 1$, the flux of A is toward the pore and is ultimately diffusion/migration limited (unless $\alpha D_A/D_B = 1$; then there is concentration polarization and no limiting current; i.e., the voltage drop will be purely ohmic). When $i/i_{\text{lim}} < 0$, the flux of A is away from the pore and is unlimited—of course, if the pore has conical access at each end as indicated in Figure 6, a flux of species A away from the pore in region 1 means that the flux of species A in region 2 must be toward the pore. A plot of $i_1/i_{\text{lim},1}$ vs $pF\Delta V/RT$ is shown in Figure 7A.

When the two cones at each end of the pore are linked, the same current flows through each cone. The voltage drop through conical region 2 is (see Appendix)

$$\Delta V_2 = -\frac{RT}{z_A pF} \ln\left[1 - \frac{i_2}{i_{\text{lim},2}}\right] \tag{10}$$

where the terms are analogous to those defined in eq 5 (the sign change occurs since potential will be computed by integrating from infinity to $r_{0,2}$; for eq 5, the integration was from $r_{0,1}$ to infinity; see Appendix). At steady state, $i_1 = -i_2$ (sign reversal occurs because our analysis assumed that a positive flux was away from the pore). Thus,

$$\Delta V_2 = -\frac{RT}{z_A pF} \ln\left[1 + \frac{i_1}{i_{\text{lim},2}}\right] \tag{11}$$

The sign convention we have imposed (Appendix, eq A11) dictates that, for conical region 1, a positive current is associated with a positive flux of a positively charged species. If we assume that the resistance R_{pore} of the pore region (see Figure 6) is ohmic, we can write

$$\Delta V_{\text{pore}} = -i_1 R_{\text{pore}} \tag{12}$$

Then, the total potential drop across the system will be

$$\Delta V_{\text{total}} = \Delta V_1 + \Delta V_2 + \Delta V_{\text{pore}} = \frac{RT}{pz_A F}\left(\ln\left[1 - \frac{i_1}{i_{\text{lim},1}}\right] - \ln\left[1 + \frac{i_1}{i_{\text{lim},2}}\right]\right) - i_1 R_{\text{pore}} \tag{13}$$

where ΔV_{total} now represents the potential applied between the two nonpolarizable electrodes in regions 1 and 2 and includes ΔV_{pore}, the potential drop in the pore region itself. For the situation under consideration here, where bulk concentrations are identical in regions 1 and 2

$$i_{\text{lim},2}/i_{\text{lim},1} = \beta_2 r_{0,2}/\beta_1 r_{0,1} \tag{14}$$

With the model proposed here, asymmetry arises because of the large difference between β_2 and β_1 and because of the permselectivity of the pore. Representative plots of the i/i_{lim} ($= i/i_{\text{lim},1}$ or $i/i_{\text{lim},2}$) vs $pz_A F(\Delta V - \Delta V_{\text{pore}})RT$ are shown in Figure 7B,C. Note that in the absence of such permselectivity, $\alpha = D_B/$

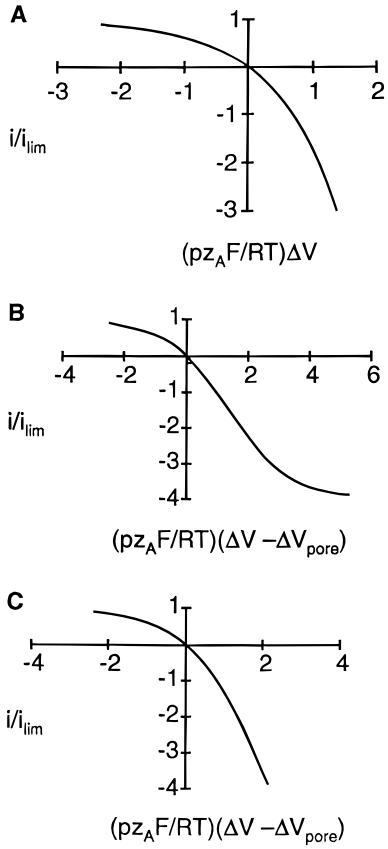

Figure 7. (A) Current−potential relationship for single cone (eqs 8 and 9) (e.g., parameters: $z_A = 1$, $z_B = 1$, $D_A = D_B = 1 \times 10^{-5}$ cm^2/s, $\alpha = 0$, $\beta = 0.2$, $C_A = 0.01$ M, $r_0 = 1 \times 10^{-6}$ cm, $p = -1$, $i_{\text{lim}} = -4.85 \times 10^{-11}$ A). (B) $i_1/i_{\text{lim},1}$−potential relationship for linked cones (eq 15) where $i_{\text{lim},2}/i_{\text{lim},1} = 4$ (e.g., parameters as in (A), with $\beta_1 = 0.2$, $\beta_2 = 0.8$, $i_{\text{lim},2} = 1.94 \times 10^{-10}$ A, and $r_{0,1} = r_{0,2} = r_0$). (C) As in (B) with $i_{\text{lim},2}/i_{\text{lim},1} = 9$.

D_A (in other words, the transference numbers for the ions through the pore and in the bulk are identical), $i_{lim} \rightarrow \infty$ (eq 7), and no asymmetry will be observed. Also note that when $i/i_{lim,1}$ and $i/i_{lim,2}$ approach zero, eq 13 linearizes to give

$$\Delta V_{total} = -i_1\left(\frac{RT}{pz_AF}\left[\frac{1}{i_{lim,1}} + \frac{1}{i_{lim,2}}\right] + R_{pore}\right) \quad (15)$$

However, permselectivity of the pore alone will not produce asymmetric behavior. It is also necessary that $\beta_1 r_1 \neq \beta_2 r_2$. For example, a highly permselective ion exchange membrane with the same solution on both sides of the membrane shows no asymmetry[13] and that is because $\beta_1 r_1 \approx \beta_2 r_2$.

While the model qualitatively can explain the observed behavior, the actual situation is probably more complicated, since convective flow (e.g., electrosmosis) could also occur during the passage of current. Moreover, surface conductivity[8] along the nanopipet capillary wall could also be significant.

CONCLUSIONS

Nonlinear current−voltage dependence has been observed at nanopipet electrodes, and we believe this to be caused by the effect of the electrical double layer at the quartz surface of the tip. This phenomenon is strongly affected by the relative dimensions of the diffuse double-layer thickness and pipet orifice and is only observed when the tip size of nanopipet electrodes is comparable to the thickness of the diffuse double layer. The results also reveal that ion transport properties through a nanopipet opening can be altered by solution pH, which affects the structure of the double layer at the quartz surface. These nanotips may be useful as models for pores with well-defined geometries in membranes. This type of structure may also be important in certain types of nanometer-sized amperometric tips, where the metallic tip is recessed within a glass or polymer substrate. By controlled modification of the tip near the orifice, selectivity may also be induced.

ACKNOWLEDGMENT

We appreciate helpful discussions with Drs. A. P. Shapiro and O. H. LeBlanc. A.J.B. gratefully acknowledges the support of this work by the National Science Foundation and the Robert A. Welch foundation. S.W.F. gratefully acknowledges the support of the Chemical Sciences Division, Office of Basic Energy Sciences, U.S. Department of Energy Contract No. DE-AC02-76CH00016.

APPENDIX: DERIVATION OF STEADY-STATE CURRENT−POTENTIAL BEHAVIOR THROUGH A CONICAL SEGMENT

Steady-State Transport to a Sphere of Radius r_0. The expressions for the fluxes of species A and B, f_A and f_B, with applicability of the Nernst−Planck equations assumed, are

$$f_A = -D_A(dC_A/dr) + D_AC_Az_A\epsilon_r \quad (A1)$$

$$f_B = -D_B(dC_B/dr) + D_BC_Bz_B\epsilon_r \quad (A2)$$

where

$$\epsilon_r = (F/RT)E_r \quad (A3)$$

and E_r is the electric field at r. From the electroneutrality condition

$$z_AC_A + z_BC_B = 0 \quad (A4)$$

and from eqs A1 and A2, we can write

$$(f_A/D_A) + (f_B/D_B) = -(dC_A/dr)[1 - (z_A/z_B)] \quad (A5)$$

From eq 4

$$f_A = -\frac{dC_A}{dr}\frac{[1 - (z_A/z_B)]}{[1/D_A - (\alpha/D_B)]} \quad (A6)$$

For a spherical geometry and steady state, we can write

$$\frac{d}{dr}\left[r^2\left(\frac{f_A}{D_A} + \frac{f_B}{D_B}\right)\right] = 0 = -[1 - (z_A/z_B)][2r(dC_A/dr) + r^2(d^2C_A/dr^2)] \quad (A7)$$

The solution is

$$C_A = C_{A,b} - (C_{A,b} - C_{A,r_0})(r_0/r) \quad (A8)$$

Differentiation of eq A8 yields

$$dC_A/dr = (C_{A,b} - C_{A,r_0})(r_0/r^2) \quad (A9)$$

and substitution into eq A6 yields

$$f_A = -\frac{[1 - (z_A/z_B)](C_{A,b} - C_{A,r_0})(r_0/r^2)}{[(1/D_A) - (\alpha/D_B)]} \quad (A10)$$

Steady-State Transport through Conical Section 1 (Figure 6). The steady-state current passing through conical region 1 (Figure 6) will be

$$i_1 = 4\pi F\beta_1 r_1^2(f_{A,1}z_A + f_{B,1}z_B) = 4\pi F\beta_1 r_1^2 f_{A,1}(z_A - \alpha z_B) \quad (A11)$$

Combining eqs A10 and A11 yields

$$i_1 = -4\pi F\beta_1 r_{0,1}D_A(C_{A,b,1} - C_{A,r_{0,1}})\frac{[1 - (z_A/z_B)](z_A - \alpha z_B)}{1 - \alpha D_A/D_B} \quad (A12)$$

When $C_{A,r_{0,1}} = 0$, $i = i_{lim,1}$, and

$$i_{lim,1} = -4\pi F\beta_1 r_{0,1}C_{A,b,1}\frac{[1 - (z_A/z_B)](z_A - \alpha z_B)}{1 - \alpha D_A/D_B} \quad (A13)$$

and

$$\frac{i_1}{i_{lim,1}} = \frac{C_{A,b,1} - C_{A,r_{0,1}}}{C_{A,b,1}} \quad (A14)$$

Note that when $\alpha = D_B/D_A$ there is no permselectivity in the pore, $i_{lim,1} \rightarrow \infty$, and $C_{A,r_{0,1}} = C_{A,b,1}$. The precisely analogous corresponding set of equations can be derived for conical region 2.

To compute the potential drop through a sphere, we reformulate eq A1 by substitution of f_A (eq A10), dC_A/dr (eq A9), and C_A

(13) Helfferich, F. *Ion Exchange*; McGraw-Hill: New York, 1962; p 397.

(eq A8), to yield

$$-\frac{[1-(z_A/z_B)](C_{A,b}-C_{A,r_0})(r_0/r^2)}{[(1/D_A)-(\alpha/D_B)]} = -D_A(C_{A,b}-C_{A,r_0})(r_0/r^2) + D_A z_A \epsilon_r [C_{A,b}-(C_{A,b}-C_{A,r_0})(r_0/r)] \quad \text{(A15)}$$

Reducing and solving for ϵ_r and substitution of eq A14 gives

$$\epsilon_r = \frac{(z_A/z_B)-\alpha(D_A/D_B)}{z_A[(i_{lim}/i)(r^2/r_0)-r][1-\alpha(D_A/D_B)]} \quad \text{(A16)}$$

The potential drop ΔV_1 through conical region 1, integrating from $r_1 = r_{0,1}$ to ∞, is

$$\Delta V_1 = -\frac{RT}{F}\int_{r_1=r_{0,1}}^{\infty} \epsilon_{r_1}\, dr_1 = \int_{r_1=r_{0,1}}^{\infty} E_{r_1}\, dr_1 \quad \text{(A17)}$$

With eq A15

$$\Delta V_1 = \frac{RT}{F}\frac{(z_A/z_B)-\alpha(D_A/D_B)}{z_A[1-\alpha(D_A/D_B)]}\ln\left[1-\frac{i_1}{i_{lim,1}}\right] \quad \text{(A18)}$$

Anticipating that potential drops through the two conical regions will be added, the potential drop ΔV_2 through conical region 2 requires that the analogous equation be integrated from $r_2 = \infty$ to $r_{0,2}$, giving

$$\Delta V_2 = -\int_{r_2=\infty}^{r_{0,2}} E_{r_2}\, dr_2 - \frac{RT}{F}\frac{(z_A/z_B)-\alpha(D_A/D_B)}{z_A[1-\alpha(D_A/D_B)]}\ln\left[1-\frac{i_2}{i_{lim,2}}\right] \quad \text{(A19)}$$

Received for review May 29, 1997. Accepted August 15, 1997.[⊗]

AC970551G

[⊗] Abstract published in *Advance ACS Abstracts*, October 1, 1997.